



Nd³⁺ ions effects on the blue emission of colloidal Y(OH)₃ nanobelts

M. M. Arghavan¹ · A. A. Sabouri-Dodaran¹ · M. Sasani Ghamsari²

Received: 15 January 2023 / Accepted: 27 June 2023 / Published online: 18 August 2023
© The Author(s), under exclusive licence to Springer Science+Business Media, LLC, part of Springer Nature 2023

Abstract

In this report, we synthesized the neodymium-doped yttrium hydroxide nanobelts (Nd:Y(OH)₃) using a facile route. The characterization methods, such as UV-Visible and photoluminescence spectroscopy, Raman, X-ray photoemission, Fourier transform infrared (FTIR) spectroscopy, and high resolution transmission electron microscopy (HRTEM), were applied to clarify the properties of the prepared colloidal sample. The structural characteristics of the prepared sample were analyzed via X-ray diffraction (XRD) and HRTEM. The average size of the hexagonal crystal is about 25 nm, which shows the compatibility of XRD and HRTEM spectroscopy results. Absorbance and emission spectra of the synthesized sample have demonstrated that the intensity of light emission by the colloidal sample is affected by the concentration of Nd³⁺ ions. In this research, it has been shown that the excitation of the samples with the wavelengths of 355 and 360 nm almost does not change the blue emission spectra because the wavelengths are related to the nature of the Nd³⁺, but with the excitation of 300 nm, the intensity of the emission spectra increases with the increase in the concentration up to 0.05 g (sample 2).

Keywords Neodymium-doped yttrium hydroxide · Nanobelts · Blue emission

1 Introduction

Rare earth elements, including yttrium, scandium, and lanthanides, have potential applications in many fields, such as medical, optical, and optoelectronic applications (Ascenzi, et al. 2020; Balaram 2019; Milanova and Tsvetkov 2021). These elements are employed in bioimaging, drug delivery, sensors, and optical devices, including displays, light-emitting

✉ A. A. Sabouri-Dodaran
sabouri@pnu.ac.ir

✉ M. Sasani Ghamsari
msasani@aeoi.org.ir

M. M. Arghavan
m.mohammadmahdi@gmail.com

¹ Department of Physics, Payame Noor University, 19395-3697 Tehran, Iran

² Photonics and Quantum Technologies Research School, Nuclear Science and Technology Research Institute, Tehran 11155-3486, Iran

diodes (LEDs), lasers, and optical amplifiers (Huang, et al. 2022; Huang, et al. 2019; Chen, et al. 2018; Ma, et al. 2019; Rosa et al. 2020; Ning et al. 2019; Zhang et al. 2017; Watanabe, et al. 2019). They are known as attractive luminescence materials due to their narrow emission band and long emission lifetime over a wide range of wavelengths (UV/Visible/NIR) (Hasegawa et al. 2018). Nowadays, rare earth elements are used in different types of oxides, hydroxide, oxysulfide, oxysulfate, oxynitride, nitrides, metal-organic frameworks (MOFs), and different complexes such as lanthanide Schiff base complexes, lanthanide azodicarboxylate compounds, or lanthanide-based hybrid materials (Khalid Hossain et al. 2021; Oliveira et al. 2021; Qian, et al. 2021; Holmes-Hewett et al. 2020; Younis et al. 2021; Saraci, et al. 2020; Taha et al. 2020; Abdel Aziz, et al. 2020; Li and Li 2021; Belousov et al. 2021; Ferreira da Rosa et al. 2020). As one of the important rare earth elements, yttrium compounds attract a lot of applications in a wide range of fields (Fisher 2004). For example, due to its high stability in air and resistance to degradation under applied voltages, europium doped yttrium oxide is known as one of the best red oxide phosphors that exhibits excellent luminescent characteristics (Zhang et al. 2017). Yttrium hydroxide with different lanthanide dopants such as Er^{3+} , Eu^{3+} , and Tb^{3+} has also attracted more attention due to its unique spectral characteristics and 4f electron orbits shielded by $5s^2$ and $5p^6$ shells of lanthanide ions (Zhu and Wang 2017). In the applications of lanthanide-doped yttrium hydroxide, its morphology is often regarded as a particularly important factor that influences its optical properties, especially when it is at the nanometer scale (Li et al. 2009). Since the optical properties of nanomaterials are affected by the preparation process, different procedures such as co-precipitation and hydrothermal methods have been explored to control the shape and dimension of yttrium hydroxide (Li et al. 2009). Among these methods, hydrothermal synthesis is known as a promising route for the preparation of one-dimensional (1D) nanostructured materials (Fang, et al. 2003). As it was previously established, the hydrothermal method can be used to synthesize 1D yttrium hydroxide nanosheets (Wang, et al. 2003). Usually, the final products coexist with a mixture of 1D $\text{Y}(\text{OH})_3$ nanostructures. For example, Wang et al. (Wang, et al. 2003), prepared a mixture of nanobelts and nanosheets of $\text{Y}(\text{OH})_3$ with very low aspect ratios using optimal pH conditions at 180 °C. Also, Fang et al. (2003) have synthesized the $\text{Y}(\text{OH})_3$ nanotubes with a little mixture of nanobelts by the hydrothermal method at 170 °C. It should be noted that in the hydrothermal method, the corresponding rare-earth oxide powders are used to synthesize the 1D nanostructures (sheet, wire, nanobelts, and tube) of $\text{Y}(\text{OH})_3$, and the presence of alkali in the hydrothermal processes is inevitable (Zhang, et al. 2008; Tat Su, et al. 2011; Hu, et al. 2007).

Due to the wide range of Nd^{3+} emission spectra in the ranges of UV, visible, and NIR, it can be used in various applications such as telecommunications, bioimaging, laser active material, anticancer activities, etc. Therefore, in this approach, we first synthesize the neodymium-doped yttrium hydroxide nanobelts using a facile route and phase (colloidal nanoparticles) that differs from other published reports (Tat Su et al. 2011; Hu et al. 2007). Then we doped different concentrations of Nd^{3+} ions in the crystal to analyze the effects of these dopant concentrations on the optical properties of the host material. In our experiments, the blue-wavelength emission was recorded from the colloidal $\text{Y}(\text{OH})_3$ nanobelts embedded with neodymium ions. Blue-wavelength light can serve in various applications such as displays and optical devices, biological fluorescence labeling, tricolor fluorescent lamps, and so on (Devi et al. 2016; Vafaei et al. 2011). The blue light emission was observed by exciting different nanoparticles such as $\text{Bi}^{3+}:\text{Y}_2\text{O}_3$ and $\text{Bi}^{3+}:\text{Y}_3\text{Al}_5\text{O}_{12}$ thin films (Devi et al. 2016), $\text{Eu}^{2+}:\text{BaMgAl}_{10}\text{O}_{17}$, $\text{Eu}^{3+}:\text{Y}_2\text{O}_3$, $\text{Dy}^{3+}:\text{Y}_2\text{O}_3$ (Bhavani et al. 2016), $\text{Yb}:\text{Y}_2\text{O}_3$ (Deshmukh et al. 2017).

2 Experimental procedure

In preparation of neodymium-doped yttrium hydroxide, first 0.1 g of yttrium oxide (Y₂O₃, Merck Co.) and 0.017 g of neodymium oxide (Nd₂O₃, Sigma-Aldrich Co.) were added to a mixed solution of absolute ethanol and deionized water, and then it was stirred at 80 °C to obtain a transparent solution. After that, 2 ml of hydrochloric acid (HCl 37%, Merck Co.) and 2 ml of acetic acid (CH₃COOH 99%, Merck Co.) were added to the precursor solution. The final solution was agitated for about 24 h to form the initial transparent colloidal sample. Then, with the same method, different colloidal samples were prepared with different Nd³⁺ ion concentrations (0.03, 0.05, and 0.1 g). Finally, the optical properties of transparent colloidal solutions have been studied by UV-Visible, photoluminescence, and FTIR spectroscopy. The shape and morphology of the colloidal sample were determined using HRTEM. To prepare the powder of neodymium-doped yttrium hydroxide, a transparent colloidal solution was dried in the oven at 70 °C. The dried powder was characterized by XRD analysis. Also, Raman spectroscopy was used for monitoring Nd³⁺ ions.

3 Result and discussion

In order to characterize the crystallinity of the colloidal sample, it was dried at 70 °C, and an X-ray diffraction pattern was applied with a PANalytical (XPerT Pro MPD) diffractometer. Figure 1 shows the XRD pattern of the prepared colloidal neodymium-doped yttrium hydroxide nanobelts with the Miller indices that were plotted using Fullprof software. It

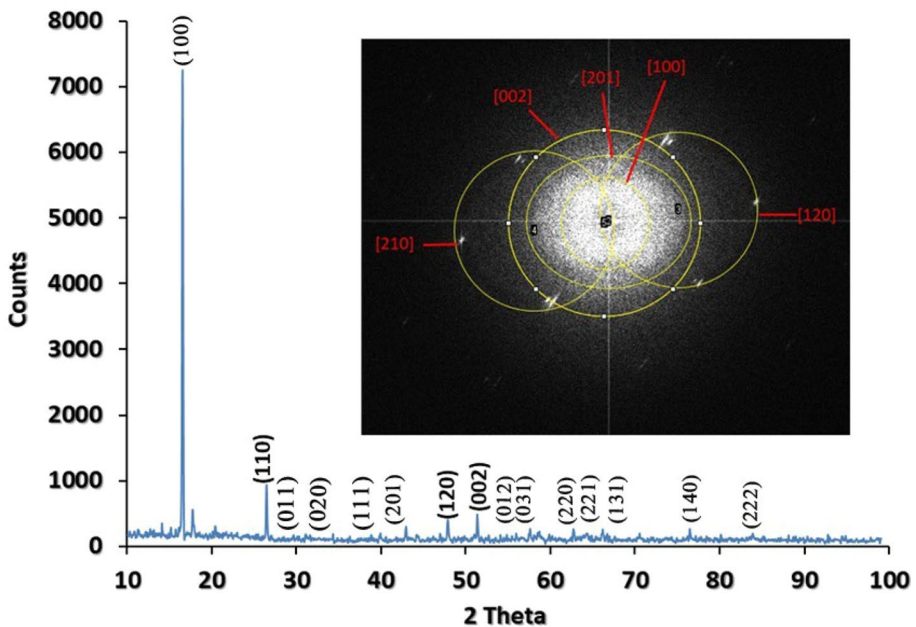


Fig. 1 XRD pattern of neodymium doped yttrium hydroxide nanobelts with the miller indices and SAED pattern

can be found from this figure that nanobelts have a hexagonal phase (space group P63/m) matched with the International Centre for Diffraction Data (ICDD) (code, which is related to yttrium hydroxide (ref. code: 00-009-0062). The six parameters of a unit cell are $a=6.26$ Å, $b=6.26$ Å, $c=3.54$ Å, $\alpha=90^\circ$, $\beta=90^\circ$, and $\gamma=120^\circ$ in which the 3 edges are; a, b, and c, and the angles between the edges are; α , β , γ . Also, according to Bragg's equation, these indices and their positions were successfully adopted with the related lattice. Also, the Scherrer equation was applied to show the crystallite size of samples (Muniz et al. 2016):

$$D = (k \times \lambda) / (FWHM \times \cos \theta) \quad (1)$$

which D is the crystallite size, k is a shape constant that is approximately equal to 0.89, and " λ " is the incident wavelength that is Cu wavelength (1.5406 Å) in this report. " θ " and FWHM are the incident angle and full width half-maximum of the diffraction peak, respectively. The average crystalline size using the highest peak of the XRD pattern is approximately 27 nm, which is consistent with the HRTEM result. In Fig. 1, an X-ray diffraction pattern is adopted with selected area electron diffraction (SAED), which has an elliptical shape because of the morphology and structure of the nanobelt (Wu et al. 2005; Shi and Li 2021; Deng et al. 2009). Selected area electron diffraction (SAED) which is attached to Fig. 1, confirms the crystallinity of the prepared sample.

The dislocation density (δ) determines the crystallinity degree of nanoparticles, which is the size of the crystal defects contained by a crystal. The relationship between crystallite size (D) and dislocation density is as follows:

$$\delta = 1/D^2 \quad (2)$$

In our research, δ approximately equals 0.04 (nm)⁻². So it shows that the Nd:Y(OH)₃ nanobelts have a high degree of crystallinity. The strain value (ϵ) of a crystal shows its alignment and is determined by the following equation:

$$\beta \cos \theta = (k\lambda/D) + 4\epsilon \sin \theta \quad (3)$$

which is the width of the full wide half-maximum (FWHM) intensity, k is a shape constant that is approximately equal to 0.89, and " λ " is the incident wavelength that is Cu wavelength (1.5406 Å) in this report. " θ " and D are the incident angle and crystallite size, respectively. In our research, ϵ approximately equals 3.2×10^{-3} , which is a very low value and shows that the Nd:Y(OH)₃ nanobelts lack strain. As the crystallite size (D) decreases, the strain value (ϵ) decreases, and the dislocation density (δ) increases (Sutapa et al. 2018; Kumar, et al. 2019).

HRTEM, as an image produced by a type of electron microscope, is used to collect the structural, chemical, and morphological information of nanomaterials, especially suspensions and colloids. To characterize the shape and size of yttrium hydroxide with a dopant of neodymium colloid nanoparticles, HRTEM was applied with FEI Tecnai G2 F20 Super-Twin TEM device with accelerating voltage of 200 kv. HRTEM images of the colloidal sample are shown in Fig. 2. As can be seen from this figure, the shape of the particles in the colloidal sample is a nanobelt with approximate width of 25 nm.

The transparent colloidal samples were analyzed by PerkinElmer. Lambda 25 UV-Visible spectrometer. So we illustrated the absorption spectrum of the prepared samples as shown in Fig. 3. As can be seen from this figure, the spectrum has five absorption peaks placed at 360, 522, 577, 740, and 794 nm. Those absorption peaks are due to the existence of Nd³⁺ ions in the host. In the following, to investigate the energy required for photoluminescence spectroscopy of the sample, it was excited with a shorter wavelength (higher

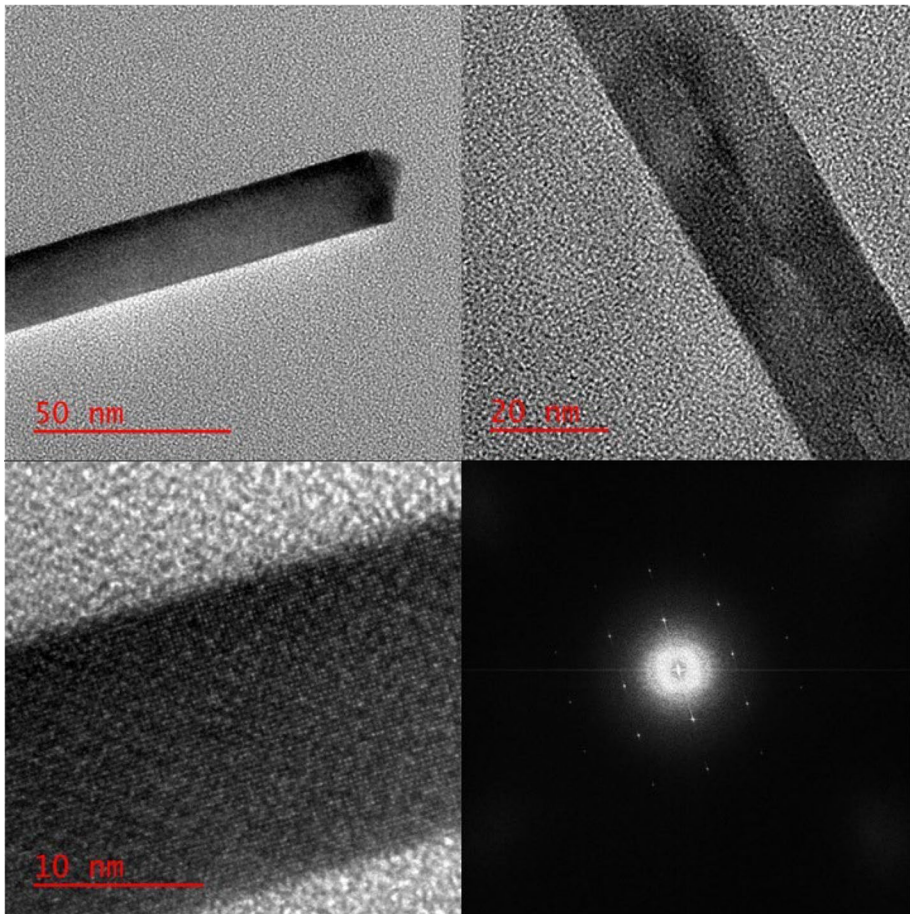


Fig. 2 HRTEM images of colloidal yttrium hydroxide with dopant of neodymium nanobelts. The diameter of the nanobelt is about 25 nm

energy) than other absorption wavelengths (300 nm). Then, the synthesized sample was excited by all the absorption peaks to create the photoluminescence spectra.

The band gap calculation of Nd:Y(OH)₃ nanobelts is done, according to the following equation and using the absorption spectrum:

$$\alpha h\nu = A(h\nu - E_g)^n \quad (4)$$

which α is the absorption coefficient, h is Planck's constant, ν is the photon's frequency, A is a constant almost equal to one at the absorption edge, E_g is the band gap, and n is an index that characterizes the optical absorption process, theoretically equal to 0.5, 1.5, 2, or 3 for direct allowed, direct forbidden, indirect allowed, and indirect forbidden transitions, respectively (Gaeeni et al. 2022; Aliakbari et al. 2020). So according to Eq. 4, for the direct allowed transition of Nd:Y(OH)₃ nanobelts, E_g equals 5.4898 eV, as shown in Fig. 4:

Figure 5 shows the best form of the emission spectra from the Avantes-Avaspec-2048 spectrometer. In Fig. 5, however, the excitation of the initial colloidal sample with

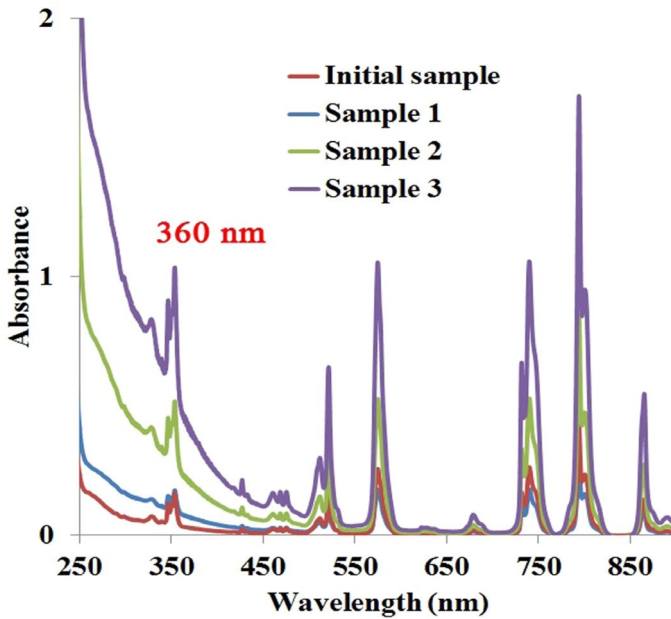


Fig. 3 Absorption spectra of the initial colloidal samples

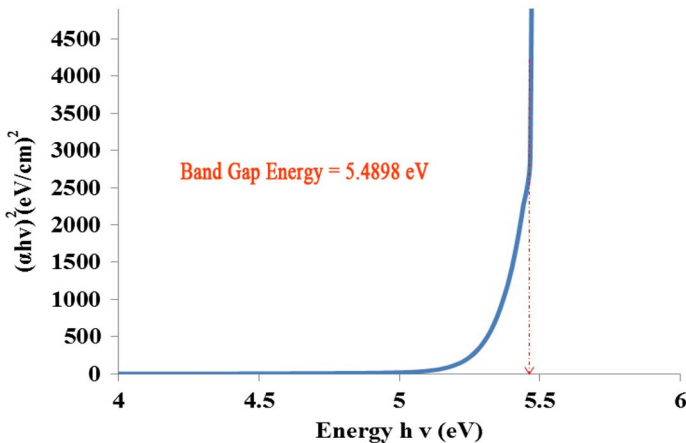


Fig. 4 $(\alpha h\nu)^2$ versus $h\nu$ plot for 0.017% Nd^{3+} doped $\text{Y}(\text{OH})_3$ nanobelts

wavelengths of 300 and 360 nm gives approximately 409 nm emission. The peak shift from blue to violet suggests the presence of defects such as the low concentration of neodymium ions and the effect of the yttrium hydroxide structure (Biju et al. 2018; Dhas et al. 2020; Jan et al. 2014). The FTIR spectrum examines the nature and purity of each chemical bond formed in the samples by identifying fluctuations. Figure 6 shows the FTIR curve that was plotted using the Bruker Alpha II FTIR spectrometer. 3427 cm^{-1} of vibration indicates the presence of the O-H bond. Carbonate and nitrate bonds are also recorded in the range of

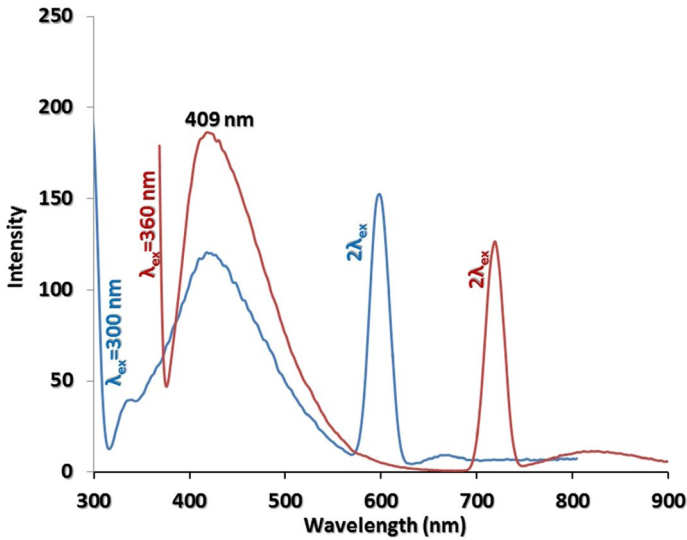


Fig. 5 Emission spectrum of the initial colloidal sample

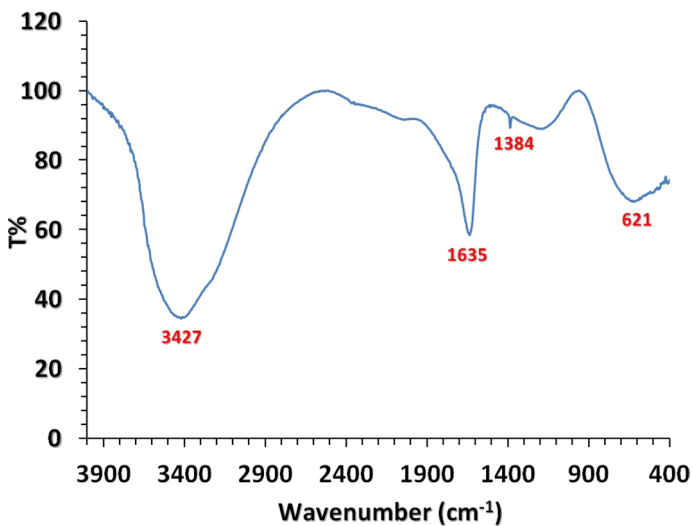


Fig. 6 FTIR spectrum of the initial colloidal sample

1590 to 1650 and 1384 cm^{-1} , respectively. 621 cm^{-1} vibration shows Y-O bonding in the sample (Nandiyanto et al. 2019; Yang et al. 2007; Aghazadeh et al. 2011).

In the following of the experiment, we characterized the three samples embedded with different concentrations of Nd³⁺ ions to show and describe the effects of various Nd³⁺ ion concentrations in photoluminescence spectra. All of them were excited by 300, 355, and 360 nm, so that all related emissions, especially the blue emission, are demonstrated. The excitation of all three samples at the wavelengths of 355 and 360 nm is approximately

equal. The reasons for the small differences include attenuation due to different concentrations, self-trapping, and scattering of energy transfer. Therefore, these wavelengths depend on the nature of the ions (neodymium) in this complex. Due to the importance of dopant concentration, only sample 2 (0.05 g) has maximum emission, and the intensities of samples 1 and 3 are approximately equal when the samples are excited by the 300 nm wavelength. Figures 7, 8 and 9 show the three emission spectra of the samples using the Avantes-Avaspec-2048 spectrometer. As seen in Fig. 9 (excitation by 360 nm) as well as Fig. 8 (excitation by 355 nm), all three samples show a blue emission spectrum. But in Fig. 7 (excitation by 300 nm), in addition to blue emission, due to higher excitation energy, violet emission was also observed. Note that there are two peaks in the excitation wavelength range, and twice of them are related to the validity of the experiment.

A commission International De'l'Eclairage (CIE) chromaticity diagram using the PL spectrum of sample 2 in Fig. 9 was prepared and shown in Fig. 10. The CIE color chromaticity coordinates are to be calculated as $(x,y) = (0.1860, 0.2814)$ using OriginPro software. It can be observed that the position of these chromaticity coordinates is located in the blue region, which shows that by careful design, Nd:Y(OH)₃ nanobelts can be applied in UV lamps and blue LEDs (Guner et al. 2019; Kumar et al. 2021).

As mentioned, blue light has various technological applications in displays and optical devices, biological fluorescence labeling, tricolor fluorescent lamps, and so on (Devi et al. 2016; Vafae et al. 2011). Hari Krishna et al. (2014) reported the photoluminescence spectra of hexagonal Y(OH)₃:Ni²⁺ and cubic Y₂O₃:Ni²⁺ nanophosphors at room

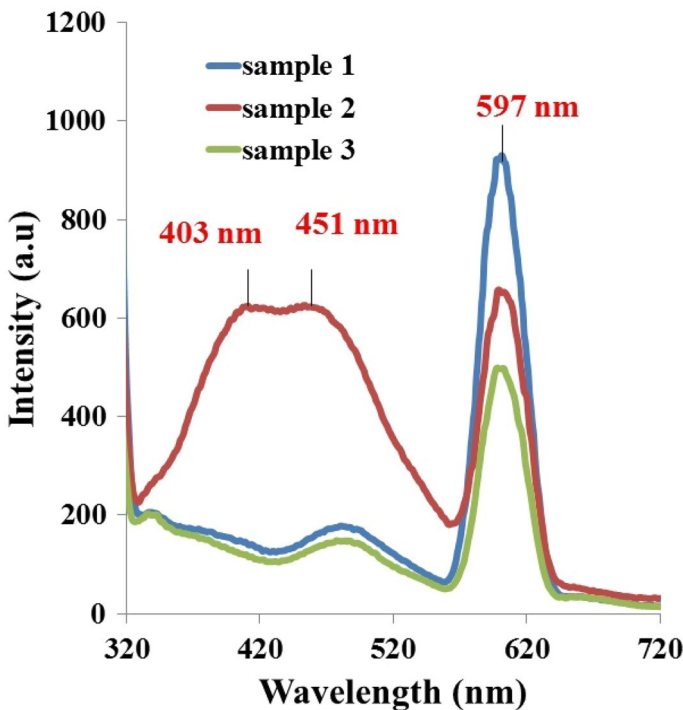


Fig. 7 PL emission spectra of the prepared sample excited by 300 nm wavelength with different Nd³⁺ concentrations respectively (0.03 g, 0.05 and 0.1 g)

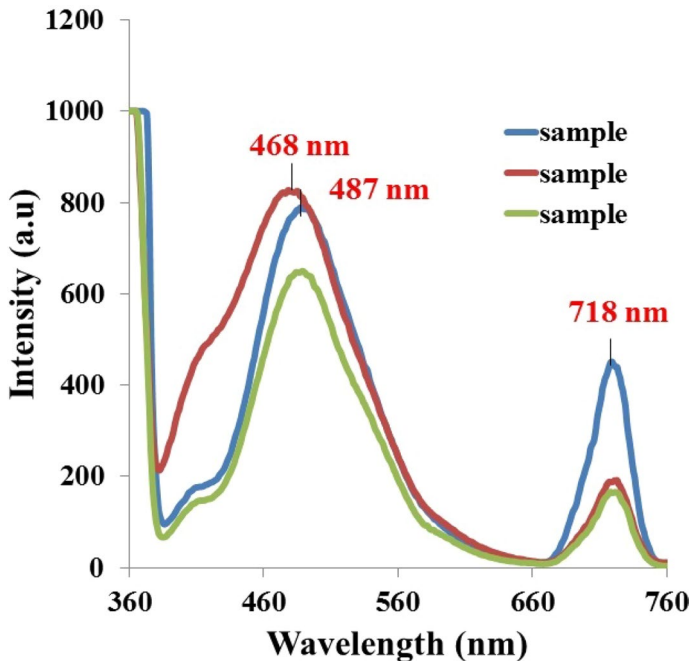


Fig. 8 PL emission spectra of the prepared sample excited by 355 nm wavelength with different Nd³⁺ concentrations respectively (0.03 g, 0.05 and 0.1 g)

temperature. Upon 306 nm excitation, they observed an intense emission at 374 nm, which can be attributed to the charge transfer band. In addition, their samples have emitted weak bands in the three regions, i.e., blue (420–485 nm), green (527 nm), and red (733 nm). At first, they stated that these emission peaks were due to the Ni²⁺ ions. The Ni²⁺ ions belong to the d⁸ configuration, and the degenerate free ion 3 F ground state of Ni²⁺ splits as a consequence of the crystal field. In an octahedral environment, the orbital singlet ³A_{2g} has the lowest energy level. They concluded that the emission in the blue, green, and red regions can be assigned to the ³T₁(³P)→³A₂(³F), ¹T₂(¹D)→³A₂(³F) and ¹T₂(¹D)→³T₂(³F) transitions of Ni²⁺ ions, respectively. However, the mechanism of blue emission in the Ln³⁺-doped host crystals is different. For Nd³⁺-doped host materials, two different mechanisms were reported for the reason of blue emission, in which high-intensity laser excitation produced emissions in the range from 400 to 500 nm due to the population of high energy levels, such as ²P_{1/2} or self-frequency doubling of the Nd³⁺, 4F_{3/2} → 4I_{9/2} laser emission (Mougel et al. 1999; Moura et al. 2015). In Nd³⁺-doped nanocrystals, the up-conversion process is very popular. This process occurs when higher-energy photons emit for the sample after the absorption of lower-energy photons (Rocha et al. 2014). In our study, we used a 325 nm excitation wavelength, and therefore, the up-conversion process could not occur. It was reported that the blue emission can be caused by self-trapped excitons (STE) (Engelsen, et al. 2016). Broad bands of intrinsic emission are related to relaxation of STE and are detected in wide-gap crystals (Lushchik et al. 2000). Previously, it was reported that the colloidal nanocrystals have the potential to emit visible light (blue) due to the trap sites, which

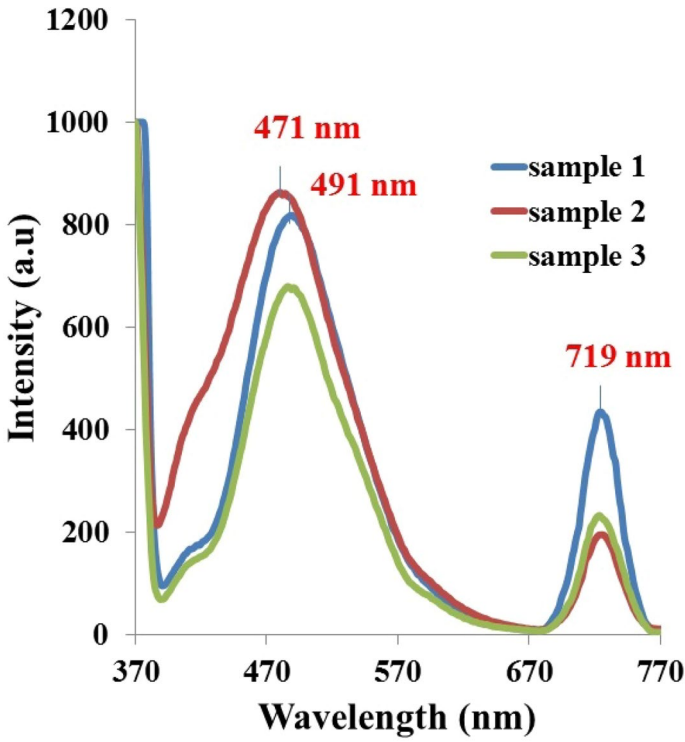


Fig. 9 Emission spectra of the prepared sample excited by 360 nm wavelength with different Nd^{3+} concentrations respectively (0.03, 0.05 and 0.1 g)

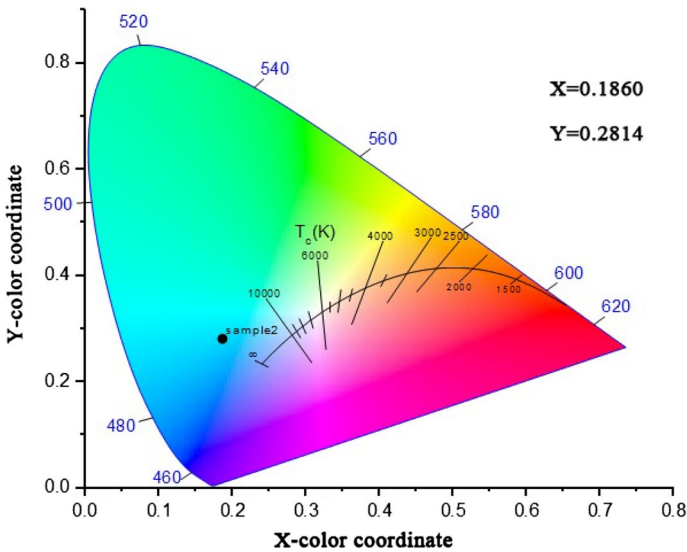


Fig. 10 CIE chromaticity coordinates of initial colloidal sample

are involved in the trapping of initially produced electron-hole pairs and are considered pathways for radiative recombination (Gaeeni, et al. 2015). Colloidal nanocrystals can also emit blue due to surface defects or oxygen vacancies (Sasani Ghamsari et al. 2016). Recently, Xie et al., (2020) prepared neodymium (III) (Nd³⁺) doped CsPbBr₃ nanocrystals through the ligand-assisted reprecipitation method at room temperature with tunable photoemission from green to deep blue with a central wavelength at 459 nm, 90% quantum yield, and a spectral width of 19 nm. They used first-principles calculations to reveal that the increase in photoluminescence quantum yield upon doping is driven by an enhancement of the exciton binding energy due to increased electron and hole effective masses and an increase in oscillator strength due to the shortening of the Pb-Br bond. Since the colloidal nanobelts were doped by Nd³⁺ ions, the recorded blue emission may be due to the down-conversion process. In the down-conversion process, the absorption of higher-energy photons (with a shorter wavelength) leads to emission with a longer wavelength than excitation photons, such as doping Nd³⁺ or Er³⁺ in nanocrystals. These processes are divided into two types: quantum cutting and downshifting (DS). In quantum cutting, a higher-energy photon is transformed into two lower-energy photons. In DS, a higher-energy photon is transformed into a longer-wavelength one, and excess energy is lost in the form of heat (Rocha et al. 2014; Osipov et al. 2009; Darshan et al. 2016).

Raman spectroscopy was applied to characterize the structural and phase transitions of materials. Figure 11 shows the Raman spectroscopy of neodymium-doped yttrium hydroxide with a Renishaw spectrometer, which is excited by 532 nm. Three peaks in 311.1 cm⁻¹, 403.9 cm⁻¹, and 483.3 cm⁻¹ are attributed to A_g translatory, E_{2g} translatory, and E_g liberation modes, respectively. These modes belong to the Raman spectra of yttrium hydroxide and confirm the hexagonal structure of the sample with a space group of P63/m. Raman

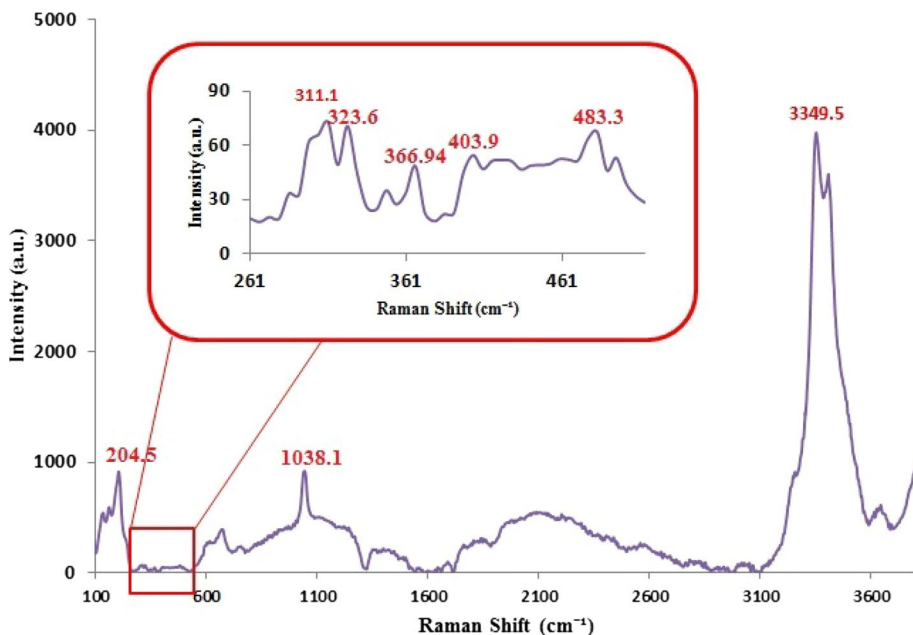


Fig. 11 Raman spectrum of neodymium-doped yttrium hydroxide nanobelts powder

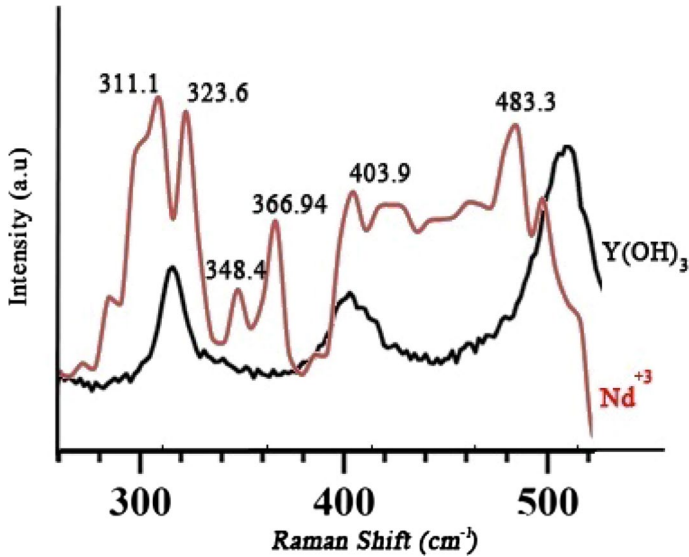


Fig. 12 The comparison between Raman spectrum of neodymium-doped yttrium hydroxide nanobelts powder (red) and Raman spectrum of yttrium hydroxide (black). 348.4 cm^{-1} , 403.9 cm^{-1} and 483.3 cm^{-1} peaks are related to Nd- translation modes and Nd-O-H bands. (Color figure online)

spectra of pure yttrium hydroxide can be found in Ref. (Gadipelly et al. 2021). A comparison between the Raman spectra of Nd:Y(OH)_3 and a pure yttrium hydroxide is shown in Fig. 12. The difference between these two plots confirms the successful neodymium doping process. Peaks that occurred in 3349.5 cm^{-1} and 366.94 cm^{-1} were also assigned to the $-\text{OH}$ band and Y-O respectively. Other peaks are related to carbonate and nitrate bands (Deshmukh et al. 2017; Gadipelly et al. 2021; Swanson et al. 1978; Guo, et al., 2009; Li et al. 2004).

4 Conclusion

In this manuscript, we synthesized the neodymium-doped yttrium hydroxide nanobelts (Nd:Y(OH)_3) and then repeated it with three different concentrations of Nd^{3+} ions. In the following, the samples were analyzed to show that this route of synthesis was completed successfully and to investigate the effect of Nd^{3+} ion concentrations. The FTIR curve of the initial sample ensures that the synthesis has been done properly. The XRD pattern of the initial sample with Miller indices confirms the structure of Y(OH)_3 . Scherrer equation and HRTEM are also applied to synthesized samples to show the dimension and morphology of the nanocrystals. Also, it was shown that their results matched. The Raman spectrum also confirms the hexagonal structure of yttrium hydroxide and shows the neodymium dopant in the sample. Absorbance and emission spectra of the synthesized sample have demonstrated that the intensity of light emission by the colloidal sample is affected by the concentration of Nd^{3+} ions. The blue emission of three samples that were excited by 350, 355, and 360 nm indicates that 355 and 360 nm wavelengths are related to the nature of the particle (neodymium), and in excitation by 300 nm wavelength, the emission intensity of sample 2 (0.05 g) is the maximum one.

Author contributions All authors wrote and reviewed the manuscript.

Funding None

Data availability All of the material is owned by the authors, and/or no permissions are required.

Declarations

Conflict of interest I declare that the authors have no competing interests as defined by Springer or other interests that might be perceived to influence the results and/or discussion reported in this paper

Ethical approval There is no ethical approval is required. 'Not Applicable'.

References

- Abdel Aziz, A.A., Sayed, M.A.: Some novel rare earth metal ions complexes: synthesis, characterization, luminescence and biocidal efficiency. *Anal. Biochem.* **598**, 113645 (2020). <https://doi.org/10.1016/j.ab.2020.113645>
- Aghazadeh, M., Ghaemi, M., Golikand, A.N., Yousefi, T., Jangju, E.: Yttrium oxide nanoparticles prepared by heat treatment of cathodically growth yttrium hydroxide. *ISRN Ceram.* 542104 (2011). <https://doi.org/10.5402/2011/542104>
- Aliakbari, A., Sasani Ghamsari, M., Mozdianfard, M.R.: β -Carbon nitride nanoflake with enhanced visible light emission. *Opt. Mater.* **107**, 110036 (2020). <https://doi.org/10.1016/j.optmat.2020.110036>
- Ascenzi, P., et al.: Rare earth elements (REE) in biology and medicine. *Rend. Lincei Scienze Fis. e Nat.* **31**, 821–833 (2020). <https://doi.org/10.1007/s12210-020-00930-w>
- Balaram, V.: Rare earth elements: a review of applications, occurrence, exploration, analysis, recycling and environmental impact. *Geosci. Front.* **10**(4), 1285–1303 (2019). <https://doi.org/10.1016/j.gsf.2018.12.005>
- Belousov, Y.A., et al.: Lanthanide azolecarboxylate compounds: structure, luminescent, properties and applications. *Coord. Chem. Rev.* **445**, 214084 (2021). <https://doi.org/10.1016/j.ccr.2021.214084>
- Bhavani, G., Ganesan, S., Selvasekarapandian, S., Monisha, S., Premalatha, M.: Synthesis and electrical characterisation of bismuth doped yttrium oxide. *Int. J. Chem. Sci.* **14**(1), 427–434 (2016)
- Biju, C.S., Suresh, S., Dhas, S.S.J., Rao, R.G.S.: Effect of lattice strain on the polychromatic emission in ZnO nanostructures for white light emitting diode application. *Superlattices Microstruct.* **120**, 363–369. (2018). <https://doi.org/10.1016/j.spmi.2018.05.064>
- Chen, W., et al.: Advances in luminescent lanthanide complexes and applications. *Sci. China Tech. Sci.* **61**, 1–21 (2018). <https://doi.org/10.1007/s11431-017-9212-7>
- Da Ferreira, P.P., Kitagawa, Y., Hasegawa, Y.: Luminescent lanthanide complex with seven-coordination geometry. *Coord. Chem. Rev.* **406**, 213153 (2020). <https://doi.org/10.1016/j.ccr.2019.213153>
- Darshan, G.P., et al.: Neodymium doped yttrium aluminate synthesis and optical properties-a blue light emitting nanophosphor and its use in advanced forensic analysis. *Dyes Pigments* **134**, 227–233 (2016). <https://doi.org/10.1016/j.dyepig.2016.06.029>
- Deng, Z., Chen, D., Tang, F., Ren, J., Muscat, A.J.: Synthesis and purple–blue emission of antimony trioxide single-crystalline nanonobelts with elliptical cross section. *Nano Res.* **2**, 151–160 (2009). <https://doi.org/10.1007/s12274-009-9014-y>
- Deshmukh, P., Satapathy, S., Ahlawat, A., Sahoo, K., Gupta, P.K.: Effect of charge transfer band on luminescence properties of Yb doped Y₂O₃ nanoparticles. *Adv. Mater. Lett.* **8**(4), 458–464 (2017). <https://doi.org/10.48550/arXiv.1601.01781>
- Devi, H.J., Singh, W.R., Loitongbam, R.S.: Red, yellow, blue and green emission from Eu⁺³, Dy⁺³ and Bi⁺³ doped Y₂O₃ nano-phosphors. *J. Fluoresc.* **26**(3), 875–889 (2016). <https://doi.org/10.1007/s10895-016-1776-5>
- Dhas, S.S.J., et al.: Effect of annealing on the photoluminescence and thermoluminescence properties of Eu⁺² doped BaSO₄ microgravel. *J. Mater. Sci. Mater. Electron.* **31**, 11113–11122 (2020). <https://doi.org/10.1007/s10854-020-03660-9>

- Engelsen, D., et al.: Ultraviolet and blue cathodoluminescence from cubic Y_2O_3 and $Y_2O_3:Eu^{+3}$ generated in transmission electron microscope. *J. Mater. Chem. C* **4**, 7026–7034 (2016). <https://doi.org/10.1039/C6TC01750A>
- Fang, Y.-P., et al.: Hydrothermal synthesis of rare earth (Tb, Y) hydroxide and oxide nanotubes. *Adv. Funt. Mater.* **13**(12), 955–960 (2003). <https://doi.org/10.1002/adfm.200304470>
- Fisher, K.J.: Scandium and yttrium. *Comp. Coord. Chem. II* (2004). <https://doi.org/10.1002/chin.200440238>
- Gadipelly, T., Dasgupta, A., Sornadurai, D., Dhara, S.: Controlling and morphology of nanocrystalline $Y(OH)_3$ powders synthesized by microwave-hydrothermal route and effect of annealing. *Appl. Phys. A* **318**, 1–7 (2021). <https://doi.org/10.1007/s00339-021-04435-7>
- Gaeni, M.R., et al.: Al_2O_3 colloidal nanocrystals with strong UV emission. *J. Am. Ceram. Soc.* **98**, 1818–1822 (2015). <https://doi.org/10.1111/jace.13546>
- Gaeni, M.R., Bakouei, A., Sasani Ghamsari, M.: Highly stable colloidal lithium niobate nanocrystals with strong violet and blue emissio. *Inorg. Chem.* **61**, 12886–12894 (2022). <https://doi.org/10.1021/acs.inorgchem.2c02143>
- Guner, T., et al.: Green fabrication of lanthanide-doped hydroxide-based phosphors: $Y(OH)_3:Eu^{+3}$ nanoparticles for white light generation. *Beilstein J. Nanotechnol.* **10**, 1200–1210 (2019). <https://doi.org/10.3762/bjnano.10.119>
- Guo, H., Qiao, Y.M.: Preparation, characterization, and strong upconversion of monodisperse $Y_2O_3:Er^{3+}, Yb^{3+}$ microspheres. *Opt. Mater.* **31**, 583–589 (2009). <https://doi.org/10.1016/j.optmat.2008.06.011>
- HariKrishna, R., et al.: Photoluminescence, thermoluminescence and EPR studies of solvothermally derived Ni^{2+} doped $Y(OH)_3$ and Y_2O_3 multi-particle-chain microrods. *J. Lumin.* **155**, 125–134 (2014). <https://doi.org/10.1016/j.jlumin.2014.06.019>
- Hasegawa, Y., Kitagawa, Y., Nakanishi, T.: Effective photosensitized, electrosensitized, and mechanosensitized luminescence of lanthanide complexes. *NPG Asia Mater.* **10**, 52–70 (2018). <https://doi.org/10.1038/s41427-018-0012-y>
- Holmes-Hewett, W.F., et al.: Nitrogen vacancies and carrier concentration control in rare-earth nitrides. *Appl. Phys. Lett.* **117**, 222409 (2020). <https://doi.org/10.1063/5.0034031>
- Hu, C., et al.: $\alpha-Fe_2O_3$ nanorings prepared by a microwave-assisted hydrothermal process and their sensing properties. *Adv. Mater.* **19**, 470–474 (2007). <https://doi.org/10.1002/adma.200601300>
- Huang, Y., et al.: Rare earth-based materials for bone regeneration: breakthroughs and advantages. *Coord. Chem. Rev.* **450**, 214236 (2022). <https://doi.org/10.1002/btm2.10262>
- Huang, H., Zhu, J.-J.: The electrochemical applications of rare earth-based nanomaterials. *Analyst* **144**, 6789–6811 (2019). <https://doi.org/10.1039/C9AN01562K>
- Khalid Hossain, M., Ishak Khan, M., El-Denglawey, A.: A review on biomedical applications, prospects, and challenges of rare earth oxides. *Appl. Mater. Today* **24**, 101104 (2021). <https://doi.org/10.1016/j.apmt.2021.101104>
- Kumar, S., et al.: Effect of silica on the ZnS nanoparticles for stable and sustainable antibacterial application. *Int. J. Appl. Ceram. Technol.* **16**, 531–540 (2019). <https://doi.org/10.1111/jiac.13145>
- Kumar, A., et al.: Highly responsive and low-cost ultraviolet sensor based on ZnS/p-Si heterojunction grown by chemical bath deposition. *Sens. Actuator A* **331**, 1–9 (2021). <https://doi.org/10.1016/j.sna.2021.112988>
- Li, P., Li, H.: Recent progress in the lanthanide-complexes based luminescent hybrid materials. *Coord. Chem. Rev.* **441**, 213988 (2021). <https://doi.org/10.1016/j.ccr.2021.213988>
- Li, W., Wang, X., Li, Y.: Single-step in situ synthesis of double bond-grafted yttrium-hydroxide nanotube core-shell structure. *Chem. Commun.* **164–165**, 164–165 (2004). <https://doi.org/10.1039/B311740E>
- Li, N., Yanagisawa, K., Kumada, N.: Facile hydrothermal synthesis of yttrium hydroxide nanowires. *Cryst. Growth Des.* **9**(2), 978–981 (2009). <https://doi.org/10.1021/cg8007798>
- Lushchik, A., Kirm, M., Lushchik, C., Martinson, I., Zimmerer, G.: Luminescence of free and self-trapped excitons in wide-gap oxides. *J. Lumin.* **87–89**, 232–234 (2000). [https://doi.org/10.1016/S0022-2313\(99\)00271-9](https://doi.org/10.1016/S0022-2313(99)00271-9)
- Ma, Q., et al.: Recent progress in time-resolved biosensing and bioimaging based on lanthanide-doped nanoparticles. *Small* **15**(32), 1–22 (2019). <https://doi.org/10.1002/sml.201804969>
- Milanova, M., Tsvetkov, M.: Rare earths doped materials. *Crystals* **11**, 231 (2021). <https://doi.org/10.3390/cryst11030231>
- Mougel, F., Aka, G., Kahn-Harari, A., Vivien, D.: CW blue laser generation by self-sum frequency mixing in $nd:Ca_4GdO(BO_3)_3$ ($nd:GdCOB$) single crystal. *Opt. Mater.* **13**, 293–297 (1999). [https://doi.org/10.1016/S0925-3467\(99\)00081-6](https://doi.org/10.1016/S0925-3467(99)00081-6)
- Moura, A.L., Jerez, V., Maia, L.J.Q., Gomes, A.S.L.: Multi-wavelength emission through self-induced second-order wave-mixing processes from a Nd^{3+} doped crystalline powder random laser. *Sci. Rep.* (2015). <https://doi.org/10.1038/srep13816>

- Muniz, F., Miranda, T.L., Dos Santos, M.A.R., Sasaki, C.M.: The Scherrer equation and the dynamical theory of X-ray diffraction. *Acta Cryst.* **72**, 385–390 (2016). <https://doi.org/10.1107/S20527331600365X>
- Nandiyanto, A.B.D., Oktiani, R., Ragadhita, R.: How to read and interpret FTIR spectroscopy of organic material. *Indones J. Sci. Technol.* **4**(1), 97–118 (2019). <https://doi.org/10.17509/ijost.v4i1.15806>
- Ning, Y., Zhu, M., Zhang, J.-L.: Near-infrared (NIR) lanthanide molecular probes for bioimaging and biosensing. *Coord. Chem. Rev.* **399**, 1–19 (2019). <https://doi.org/10.1016/j.ccr.2019.213028>
- Oliveira, N.A., Bispo-Jr, A.G., Shinohara, G.M.M., Lima, S.A.M., Pires, A.M.: The influence of the complexing agent on the luminescence of multicolor-emitting Y₂O₃:Eu³⁺, Er³⁺, Yb³⁺ phosphors obtained by the Pechini's method. *Mater. Chem. Phys.* **257**, 123840 (2021). <https://doi.org/10.1016/j.matchemphys.2020.123840>
- Osipov, V.V., Solomonov, V.I., Spirina, A.V., Ivanov, M.G., Orlov, A.N.: Luminescence of neodymium-doped yttria. *Opt. Spectrosc.* **106**(1), 78–83 (2009). <https://doi.org/10.1364/JOT.78.000408>
- Qian, B., et al.: Comparative study on the morphology, growth mechanism and luminescence property of RE₂O₃:Eu³⁺ (RE = Lu, Gd, Y) phosphors. *J. Alloys Compd.* **870**, 159273 (2021). <https://doi.org/10.1016/j.jallcom.2021.159273>
- Rocha, U., et al.: Neodymium-doped LaF₃ nanoparticles for fluorescence bioimaging in second biological window. *Small* **6**, 1141–1154 (2014). <https://doi.org/10.1002/sml.201301716>
- Rosa, P.P.F., Kitagawa, Y., Hasegawa, Y.: Luminescent lanthanide complex with seven coordination geometry. *Coord. Chem. Rev.* **406**, 1–9 (2020). <https://doi.org/10.1016/j.ccr.2019.213153>
- Saraci, F., Quezada-Novoa, V., Donnarumma, P.R., Howarth, A.J.: Rare-earth metal–organic frameworks: from structure to applications. *Chem. Soc. Rev.* **49**(22), 7949–7977 (2020). <https://doi.org/10.1039/D0CS00292E>
- Sasani Ghamsari, M., Gaeni, M.R., Han, W., Park, H.H.: Highly stable colloidal TiO₂ nanocrystals with strong violet–blue emission. *J. Luminesc.* **178**, 89–93 (2016). <https://doi.org/10.1016/j.jlumin.2016.05.036>
- Shi, H.-L., Li, Z.-A.: Unitcell tools, a package to determine unit-cell parameters from a single electron diffraction pattern. *IUCrJ* **8**, 805–813 (2021). <https://doi.org/10.1107/S2052252521007867>
- Sutapa, I.W., Wahab, A.W., Taba, P., Nafie, N.L.: Dislocation, crystallite size distribution and lattice strain of magnesium oxide nanoparticles. *J. Phys. Conf. Ser.* **979**, 1–10 (2018). <https://doi.org/10.1088/1742-6596/979/1/012021>
- Swanson, B.L., Machell, C., Beall, G.W., Milligan, W.O.: Vibrational spectra and assignments for the lanthanide trihydroxides. *J. Inorg. Nucl. Chem.* **40**(4), 694–696 (1978). [https://doi.org/10.1016/0022-1902\(78\)80391-1](https://doi.org/10.1016/0022-1902(78)80391-1)
- Taha, Z.A., Hijazi, A.K., Al Momani, W.M.: Lanthanide complexes of the tridentate Schiff base ligand salicylaldehyde-2-picolinoylhydrazone: synthesis, characterization, photophysical properties, biological activities and catalytic oxidation of aniline. *J. Mol. Struct.* **1220**, 128712 (2020). <https://doi.org/10.1016/j.molstruc.2020.128712>
- Tat Su, L., et al.: High index, reactive facet-controlled synthesis of one-dimensional single crystalline rare earth hydroxide nanobelts. *Cryst. Eng. Commun.* **13**, 5367–5373 (2011). <https://doi.org/10.1039/C1CE05357D>
- Vafaei, M., Sasani Ghamsari, M., Radiman, S.: Highly concentrated zinc oxide nanocrystals sol with strong blue emission. *J. Luminesc.* **131**, 155–158 (2011). <https://doi.org/10.1016/j.jlumin.2010.09.042>
- Wang, X., Li, Y.: Rare earth-compounds nanowires, nanotubes, and fullerene-like nanoparticles: synthesis, characterization and properties. *J. Chem. Eur.* **9**, 5627–5635 (2003). <https://doi.org/10.1002/chem.200304785>
- Watanabe, N., et al.: Multiple color inorganic thin-film phosphor, RE-doped amorphous gallium oxide (RE = rare earth: Pr, Sm, Tb, and Dy), deposited at room temperature. *Phys. Status Solidi A* **216**, 1700833 (2019). <https://doi.org/10.1002/pssa.201700833>
- Wu, X., Tao, Y., Gao, F., Dong, L., Hu, Z.: Preparation and photoluminescence of yttrium hydroxide and yttrium oxide doped with Europium nanowires. *J. Cryst. Growth* **277**, 643–649 (2005). <https://doi.org/10.1016/j.jcrysgro.2005.01.098>
- Xie, Y., et al.: Highly efficient blue-emitting CsPbBr₃ perovskite nanocrystals through neodymium doping. *Adv. Sci.* **7**(20), 1–9 (2020). <https://doi.org/10.1002/advs.202001698>
- Yang, L., May, P.W., Yin, L., Smith, J.A., Rosser, K.N.: Ultra-fine carbon nitride nanocrystals synthesized by laser ablation in liquid solution. *J. Nanopart. Res.* **9**, 1181–1185 (2007). <https://doi.org/10.1007/s11051-006-9192-4>
- Younis, S.A., Bhardwaj, N., Bhardwaj, S.K., Kim, K.-H., Deep, A.: Rare earth metal–organic frameworks (RE-MOFs): synthesis, properties, and biomedical applications. *Coord. Chem. Rev.* **429**, 213620 (2021). <https://doi.org/10.1016/j.ccr.2020.213620>

- Zhang, N., et al.: Selective and controlled synthesis of single-crystalline yttrium hydroxide/oxide nanosheets and nanotubes. *J. Phys. Chem. C*. **112**(46), 17788–17795 (2008). <https://doi.org/10.1021/jp803831g>
- Zhang, K., Kleit, A.N., Nieto, A.: An economics strategy for criticality–application to rare earth element yttrium in new lighting technology and its sustainable availability. *Renew. Sust Energ. Rev.* **77**, 899–915 (2017). <https://doi.org/10.1016/j.rser.2016.12.127>
- Zhu, Q., Wang, X., Li, J.-G.: Recent progress in layered rare-earth hydroxide (LRH) and its application in luminescence. *J. Adv. Ceram.* **6**, 177–186 (2017). <https://doi.org/10.1007/s40145-017-0238-0>

Publisher's Note Springer Nature remains neutral with regard to jurisdictional claims in published maps and institutional affiliations.

Springer Nature or its licensor (e.g. a society or other partner) holds exclusive rights to this article under a publishing agreement with the author(s) or other rightsholder(s); author self-archiving of the accepted manuscript version of this article is solely governed by the terms of such publishing agreement and applicable law.